

Magnetic phase diagram, critical behavior, and two-dimensional to three-dimensional crossover in the triangular lattice antiferromagnet $\text{RbFe}(\text{MoO}_4)_2$

L. E. Svistov, A. I. Smirnov, and L. A. Prozorova

P. L. Kapitza Institute for Physical Problems RAS, 117334 Moscow, Russia

O. A. Petrenko

Department of Physics, University of Warwick, Coventry, CV4 7AL, United Kingdom

A. Micheler and N. Büttgen

Experimentalphysik V, Center for Electronic Correlations and Magnetism, University of Augsburg, D-86135 Augsburg, Germany

A. Ya. Shapiro and L. N. Demianets

A. V. Shubnikov Institute for Crystallography RAS, 117333 Moscow, Russia

(Received 22 March 2006; revised manuscript received 29 May 2006; published 17 July 2006)

We have studied the magnetic and thermodynamic properties as well as the NMR spectra of the quasi-two-dimensional (quasi-2D) Heisenberg antiferromagnet $\text{RbFe}(\text{MoO}_4)_2$. The observed temperature dependence of the order parameter, the critical indices, and the overall magnetic H - T phase diagram are all in a good agreement with the theoretical predictions for a 2D XY model. The temperature dependence of the specific heat at low temperature demonstrates a crossover from a T^2 law characteristic of a two-dimensional antiferromagnet to a three-dimensional T^3 law.

DOI: [10.1103/PhysRevB.74.024412](https://doi.org/10.1103/PhysRevB.74.024412)

PACS number(s): 75.50.Ee, 76.60.-k

I. INTRODUCTION

The problem of finding the ground state of a two-dimensional triangular lattice antiferromagnet (TLAM) is of particular interest due to the possibility of finding solutions with unconventional magnetic order, which are influenced significantly both by frustration and by zero-point fluctuations. As the magnetic exchange interactions between the ions located on a regular two-dimensional (2D) triangular lattice are frustrated, a usual Néel-type ground state with antiparallel alignment of the nearest-neighbor moments is hindered by the geometry. In the molecular field approximation, the minimum of energy is reached for a planar spin configuration with the magnetization of the three sublattices arranged at 120° to one other. Such a spin configuration has been found in numerous compounds with a stacked triangular lattice,¹ regardless of the dimensionality of the magnetic interactions, which can have a pronounced 1D or 2D character. A very recent report suggests that instead of a long-range structure, a spin-liquid state with a relatively short correlation length may be stabilized in some compounds.²

In an applied magnetic field, the mean-field ground state of the 2D triangular antiferromagnet is highly degenerate, as the overall energy is defined only by the total spin of the three sublattices, while there is an infinitely large number of different states with the same total spin.^{3,4} Indeed, any possible value of the total spin can be represented as an umbrella-type structure of equally tilted magnetic moments with identical transverse components or, alternatively, as a variety of both planar and nonplanar structures with variable angles between the magnetic moments and the direction of the field.

This degeneracy is removed by thermal and quantum fluctuations, which select a symmetric planar structure for a

purely isotropic (Heisenberg) case, for an easy-axis type of anisotropy and also for an easy-plane type of anisotropy if the field is applied in the basal plane.⁵⁻⁸ If the field is applied perpendicular to the easy plane, the mean-field approach yields an umbrella-type structure, which is nondegenerate with respect to the mutual orientation of magnetic moments. For the planar structures, fluctuation analysis reveals a characteristic feature of the magnetization curve $M(H)$: namely, a collinear magnetic structure with nearly one-third of the saturation magnetization ($M = M_s/3$) that is stabilized by the fluctuations in the vicinity of the field $H_s/3$, where H_s is the saturation field. The stabilization of this structure is seen as a plateau on the $M(H)$ curve, while in the molecular field approximation the magnetization curve has a continuous derivative. This structure is referred to as “two spins up, one down” or UUD.

Apart from this, TLAM's are distinguished from conventional collinear ferromagnets and antiferromagnets by the fact that for some phases, called *chiral* phases, there are still two ways to arrange the rest of the structure even when the direction of the spin on a particular apex of the triangle is fixed. Figure 1 shows two magnetic structures a and b , which share the alignment of the spin in the position A and possess the same exchange energy, but differ by the direction of rotation of the spins when translated to the nearest apex. Chiral degeneracy influences considerably the nature of the phase transition to an ordered state.^{3,9} Within a magnetic H - T phase diagram for a single TLAM, both chiral and nonchiral structures are possible; therefore, the second-order phase transitions with different critical indices should be expected for the different values of an applied magnetic field.

An especially interesting point to consider is a transition from a paramagnetic phase to a UUD structure occurring in a constant field on lowering the temperature. This is a transi-

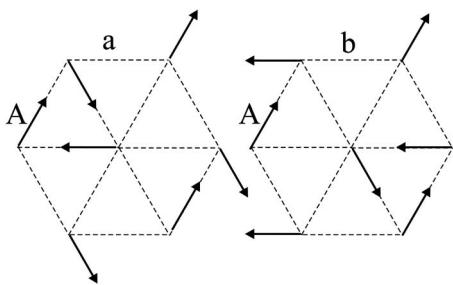


FIG. 1. Two different magnetic structures on a hexagonal lattice possessing the same exchange energy. The direction of magnetic moment at point A is identical for both structures.

tion into a collinear phase with an uncompensated magnetic moment. Such structures with uncompensated magnetic moment are characteristic of ferrimagnets; therefore, for a description of this collinear phase on a triangular lattice a ferrimagnetic order parameter is used.⁹ In ordinary ferrimagnets, however, the magnetic ions are located on non-equivalent crystallographic positions, which leads to the appearance of nonequivalent magnetic sublattices and an uncompensated moment. In these conventional ferrimagnets an ordering transition in an applied magnetic field is absent, as an induced moment exists at all temperatures. In the case of a 2D TLAM, however, all the magnetic ions are in equivalent positions, while the ordering into a UUD structure is accompanied by a tripling of the unit cell area, which causes a transition of a specific type.⁴

The majority of TLAM's have quasi-one-dimensional character. These systems have been known and studied for some time now.¹ Two-dimensional TLAM's demonstrating the properties described above are less common and have only recently become the subject of intense investigations. $\text{RbFe}(\text{MoO}_4)_2$ offers a rare opportunity to study a model system, which resembles closely an ideal 2D TLAM. The crystal structure of $\text{RbFe}(\text{MoO}_4)_2$ described by the space group D_{3d}^3 consists of layers of magnetic Fe^{3+} ions separated by $(\text{MoO}_4)^{2-}$ groups and Rb^+ ions. The C^3 axis is perpendicular to the layers. The magnetic Fe^{3+} ions form an equilateral triangular lattice within the layers, whereas along the C^3 axis they are interspaced by the Rb^+ ions. Such a layered structure (depicted in Refs. 10 and 11) ensures the magnetic two-dimensionality of $\text{RbFe}(\text{MoO}_4)_2$.^{10,12}

Relatively weak exchange interactions in $\text{RbFe}(\text{MoO}_4)_2$ allow one to reach the saturation field experimentally, while the large spin ($S=5/2$) of the magnetic Fe^{3+} ions justify a quasiclassical description of the magnetic system. Previous experiments on powder and single-crystal samples of $\text{RbFe}(\text{MoO}_4)_2$ established the presence of long-range magnetic order below $T_N=3.8$ K and also demonstrated the stabilization of the collinear structure around $M_s/3$.^{12,13} Specific heat measurements¹⁴ gave estimates of the magnetic entropy change during the ordering process. The dynamics of low-frequency excitations probed by electron spin resonance (ESR) measurements¹² gave an estimate for the ratio of the intraplane to interplane exchange interactions as 25 and were also used to evaluate the magnetic anisotropy. By measuring the field and temperature dependence of the magnetization¹²

and the specific heat,¹⁴ the magnetic H - T phase diagram was mapped out, the overall shape of which agreed well with the theoretical predictions for a 2D TLAM.^{3,4,8,9}

Neutron diffraction measurements performed in zero field¹⁵ have found an ordered structure with a tripled in-plane period, which corresponds to a 120° configuration within the layers and an incommensurate ordering along the C^3 axis. NMR spectra of the ^{87}Rb ions located between the magnetic Fe^{3+} ions from neighboring planes were reported in Ref. 16. These spectra have allowed identification of various low-temperature phases: a structure with incommensurate modulation along the C^3 axis in low fields, a tilted commensurate structure, and a UUD structure in higher fields.

This paper presents the results of a detailed investigation of the magnetic phase diagram and critical behavior in the different phases of $\text{RbFe}(\text{MoO}_4)_2$ obtained by thermodynamic measurements. It also reports on the temperature dependence of the order parameter obtained by the ^{87}Rb NMR spectroscopy. The magnetic properties, phase diagram, and critical indices demonstrate good quantitative agreement with the theoretical predictions for a classical 2D XY model.

II. EXPERIMENTAL DETAILS

Single-crystal samples of $\text{RbFe}(\text{MoO}_4)_2$ were synthesized by means of spontaneous crystallization as described in Ref. 10. The samples were thin (0.5 mm), nearly hexagonal plates with lengths along the edges up to 6 mm. The C^3 axis was found to be perpendicular to the surface of the plates for all samples. The results reported in this paper were obtained using samples produced by a significantly slower cooling of the melt compared to the samples used in Refs. 12 and 14 (1 K/h vs 3 K/h). This has resulted in samples with increased thickness and linear dimensions.

The magnetic moment was measured in a field of up to 12 T using an Oxford Instruments vibrating sample magnetometer. The heat-capacity measurements were performed by the standard heat-pulse method in the temperature range 0.4 to 40 K in a field of up to 9 T using a Quantum Design PPMS calorimeter equipped with a ^3He option. NMR spectra of the ^{87}Rb ions ($I=3/2$, $\gamma=13.9312$ MHz/T) were recorded on the homemade spectrometer covering the range 35–114 MHz. The spin-echo signal was observed at constant frequency on sweeping the magnetic field in the range 2.5–9 T. Radio frequency pulses of $5 \mu\text{s}$ and $10 \mu\text{s}$ were separated by the time interval $\tau_D=50 \mu\text{s}$.

III. EXPERIMENTAL RESULTS

A. Magnetization and specific heat measurements

The field and temperature dependences of the magnetic moment of $\text{RbFe}(\text{MoO}_4)_2$ are shown in Figs. 2 and 3 respectively. The $M(H)$ and especially the dM/dH curves show a strong decrease of the $M(H)$ slope in a field range (H_{c1}, H_{c2}) around the point where $M=M_s/3$, as well as an additional phase transition at H_{c3} accompanied by a weak hysteresis. The obtained data are very similar to the $M(H)$ curves reported previously,¹² apart from slightly reduced hysteresis

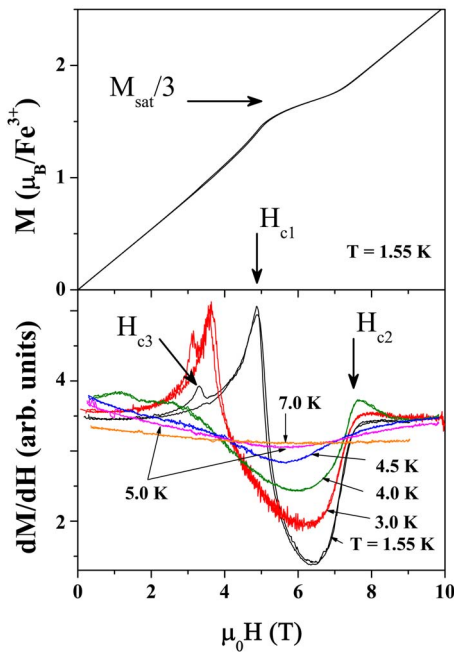


FIG. 2. (Color online) Magnetization curve versus field of a RbFe(MoO₄)₂ single crystal at $T=1.55$ K (top panel) and the derivative $\frac{dM}{dH}$ taken at different temperatures (bottom panel). The field is applied perpendicular to the C^3 axis.

effects around the H_{c3} field and also a small (about 0.1 K) increase in the ordering temperature compared to the value of T_N obtained on the batch of the samples studied beforehand.^{12,14,15} For this new sample batch, the relative amplitude of the susceptibility peak at T_N has increased by a factor of 2 for small applied fields, which usually indicates an improved sample quality. The anomalies, singularities, and other special points, which are seen in the curves in Figs. 2 and 3 and which correspond to various phase transitions, are used to locate the positions of the phase boundaries, which are later summarized in the magnetic phase diagram (Fig. 11).

Figure 4 shows the temperature dependence of the specific heat measured in RbFe(MoO₄)₂ for various values of a magnetic field applied in the basal plane of the crystal. The $C(T)$ curves demonstrate sharp anomalies corresponding to

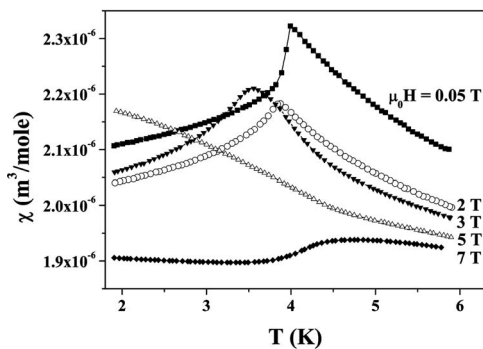


FIG. 3. Temperature dependence of the magnetic susceptibility of a single crystal of RbFe(MoO₄)₂, $\mathbf{H} \perp C^3$, measured in different magnetic fields.

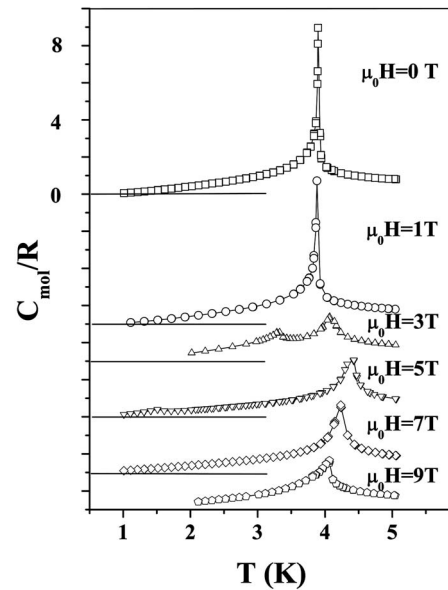


FIG. 4. Temperature dependence of the specific heat measured in RbFe(MoO₄)₂, $\mathbf{H} \perp C^3$, measured in different magnetic fields. The curves are offset along the vertical axis.

the phase transition from the high-temperature paramagnetic phase to the low-temperature magnetically ordered phase in every field from 0 to 9 T. For the $C(T)$ curves measured in the field interval 2.5–5.5 T, additional peaks are also observed when the external field coincides with the value of H_{c1} .

Figure 5 shows the field dependence of the specific heat measured at different temperatures ($\mathbf{H} \perp C^3$). For temperatures below 4 K, sharp peaks associated with the start of the plateau at H_{c1} are clearly seen on the $C(H)$ curves, while the phase transitions at H_{c2} or H_{c3} could not be detected here. For temperatures above 4.5 K, a wide and round maximum in $C(H)$ develops around a field of 5 T. On further heating, this maximum reduces in amplitude and becomes undetectable above 8 K. The observed peak positions were plotted on the phase diagram (Fig. 11) together with the data obtained from the magnetization measurements.

As can be seen from Fig. 4, the application of a weak magnetic field reduces marginally the ordering temperature. However, when the field is strong enough to stabilize a collinear phase, the ordering temperature develops a nonmono-

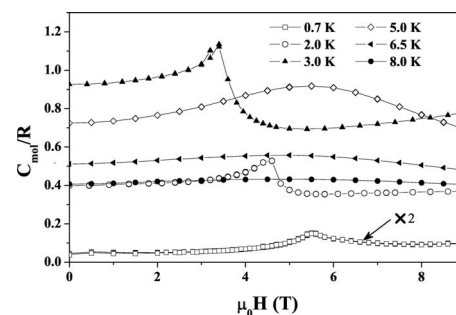


FIG. 5. Field dependence of the specific heat of RbFe(MoO₄)₂ measured for $\mathbf{H} \perp C^3$ for various temperatures.

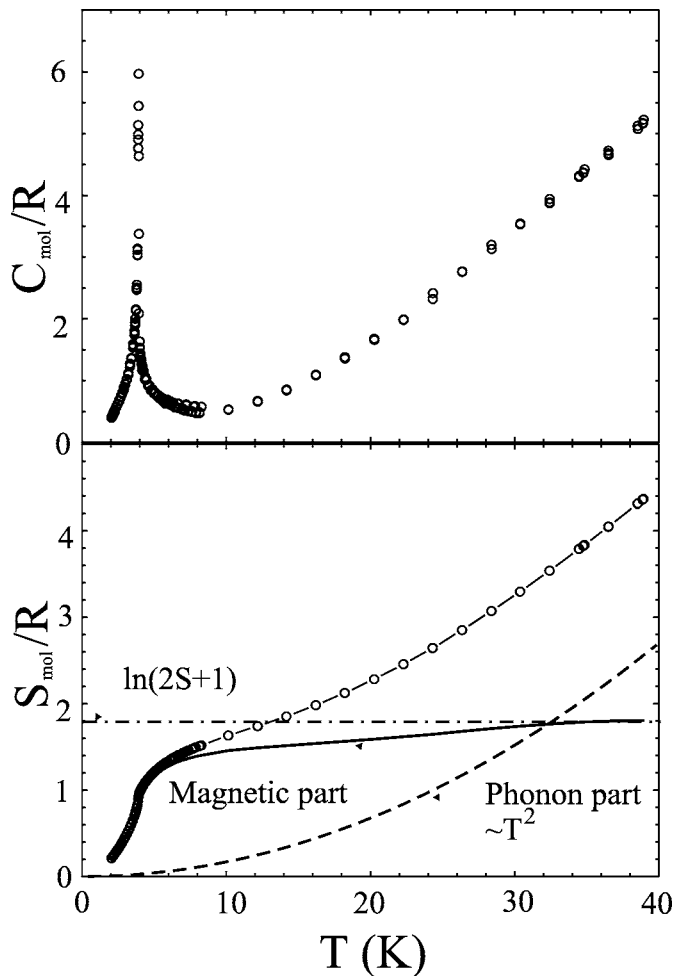


FIG. 6. Temperature dependence of the specific heat (top panel) and the entropy (bottom panel) measured in $\text{RbFe}(\text{MoO}_4)_2$ in zero field. The dashed and solid lines correspond to the lattice and magnetic contributions to the entropy.

tonic dependence with applied field. It rises with field for $H > H_{c1}$ reaching a maximum of 4.5 K at $H = 5$ T. This maximum value exceeds significantly the zero-field ordering temperature of 3.9 K.

The top panel of Fig. 6 shows the temperature dependence of the specific heat measured in $\text{RbFe}(\text{MoO}_4)_2$ for a wide temperature interval in zero magnetic field. For temperatures in the region 10–40 K, the specific heat follows a T^2 -type of the temperature dependence. As this dependence is observed both below and above the Weiss temperature, $\theta_{CW} = 25$ K, it is reasonable to suggest that it corresponds mostly to lattice vibrations. Extrapolation of the lattice contribution down to zero temperature shows that for $T < 5$ K, the magnetic contribution to the specific heat is dominant and that the lattice contribution can be neglected. The temperature dependence of the entropy obtained by integrating the $C(T)/T$ vs T curves is shown in the bottom panel of Fig. 6. By subtracting the lattice contribution (the dashed line) one can obtain the temperature dependence of the magnetic entropy, shown in Fig. 6 as a solid line. At temperatures exceeding several times the ordering temperature T_N the magnetic entropy tends to a value agreeing well with $R \ln(2S+1) = R \ln 6$.

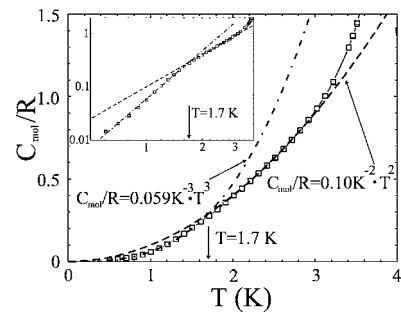


FIG. 7. Temperature dependence of the specific heat of $\text{RbFe}(\text{MoO}_4)_2$ in the low-temperature region. A crossover from a square to a cubic temperature dependence is clearly visible on the log-log plot (the inset).

Figure 7 shows temperature dependence of the zero-field specific heat of $\text{RbFe}(\text{MoO}_4)_2$ in the low-temperature region. For $T < 1.7$ K the temperature dependence of the specific heat is described well by the regular cubic law (shown by the dash-dotted line in Fig. 7), while in the temperature interval 1.7–3.4 K it follows a quadratic dependence (shown by the dashed line). The inset in Fig. 7 reproduces the same data on a double-logarithmic scale.

B. NMR ^{87}Rb spectra

The NMR ^{87}Rb spectra were recorded in the frequency range 35–115 MHz for various temperatures. The typical temperature evolution of the spectra is illustrated in Fig. 8, where the top panel shows the field dependence of the spin-echo signal at different temperatures and the bottom panel shows the temperature dependence of the resonance fields. In the paramagnetic phase, the NMR spectrum consists of three lines, with the central line corresponding to the $(-1/2 \leftrightarrow 1/2)$ transition and the two satellites to the $(-3/2 \leftrightarrow -1/2)$ and $(1/2 \leftrightarrow 3/2)$ transitions. The frequency difference for these transitions is caused by the quadrupole splitting, which is found to be temperature independent over the entire temperature range under investigation. The description and interpretation of the NMR spectra in $\text{RbFe}(\text{MoO}_4)_2$ and also their relation with the magnetic structure are given in our earlier paper.¹⁶ As was shown in that paper, the value of the NMR frequency in $\text{RbFe}(\text{MoO}_4)_2$ is determined mostly by the external magnetic field, by the quadrupole splitting, and also by the dipolar field created by the magnetic Fe^{3+} ions on ^{87}Rb nuclei, while the contribution from the hyperfine field is negligibly small.

In the paramagnetic phase, on lowering the temperature, all three NMR lines shift slightly towards higher fields and also broaden while approaching the ordering temperature T_N . The shift is caused by the dipolar field created on Rb sites by the field-induced magnetic moments of the Fe^{3+} ions.

In the magnetically ordered phases, the dipolar fields of the Fe ions make the Rb ion positions nonequivalent, which results in a splitting of all the spectral components into pairs of lines with distinct intensity. The more intense line shifts towards lower field, while the less intense line shifts towards higher field. The ratio of the intensities for these lines is

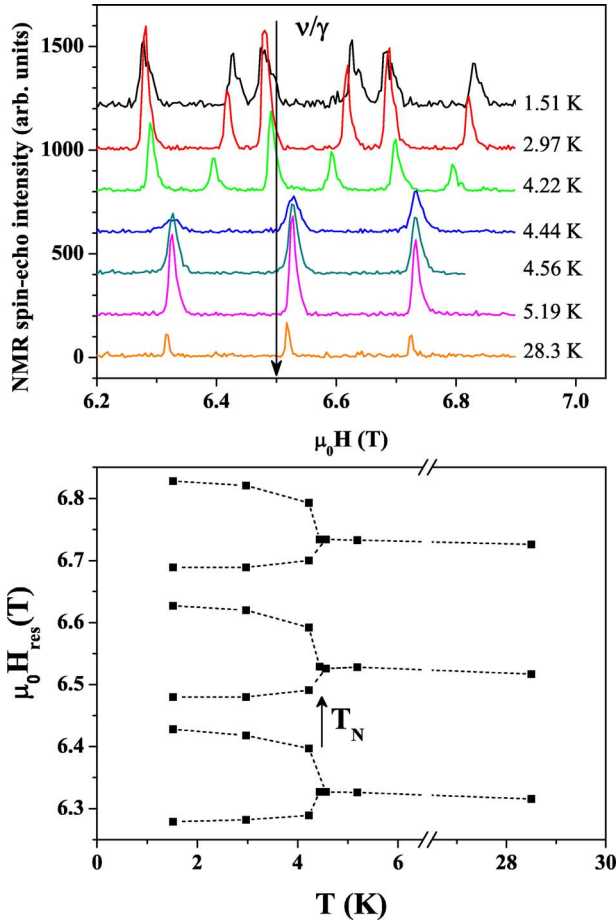


FIG. 8. (Color online) NMR spectra of $\text{RbFe}(\text{MoO}_4)_2$ recorded for a frequency of 90.6 MHz at various temperatures, $\mathbf{H} \perp C_3$ (top panel). Bottom panel shows the temperature dependence of the resonance fields.

approximately 2 to 1. The observed splitting can be used for a precise determination of the Néel temperature; it is also useful in choosing an appropriate model for the magnetic structure of $\text{RbFe}(\text{MoO}_4)_2$.¹⁶ The values of the ordering temperatures, as inferred from the NMR results, are also collected in Fig. 11, below, together with the magnetization and specific heat points.

In order to determine the temperature dependence of the order parameter, detailed NMR measurements were performed near the critical temperature for one of the spectral components. This component is seen at a frequency of 81 MHz in a field of 5.82 T, which is nearly in the center of the collinear phase. The values of the resonance fields for a central line above and below its splitting point are plotted in Fig. 9.

Let us define here the order parameter in the collinear phase following Ref. 17:

$$\eta = [(\mathbf{M}_1 + \mathbf{M}_2)/2 - \mathbf{M}_3]/2, \quad (1)$$

where \mathbf{M}_1 , \mathbf{M}_2 , and \mathbf{M}_3 are the magnetic moments of the three sublattices normalized per magnetic ion. The parameter η is zero in the paramagnetic phase and nonzero in the or-

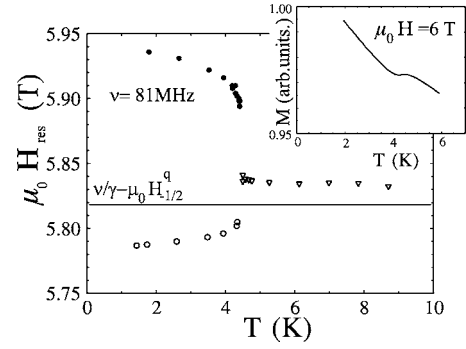


FIG. 9. Temperature dependence of the NMR resonance field $B_{res}(T)$ and the magnetic moment $M(T)$. $\mu_0 H \approx 6$ T, $\mathbf{H} \perp C_3$.

dered collinear phase. Let us also introduce a normalized full magnetic moment

$$\mu = (\mathbf{M}_1 + \mathbf{M}_2 + \mathbf{M}_3)/3. \quad (2)$$

The temperature dependence of the order parameter η can be established by measuring the local field B_{eff} , which is created by the Fe^{3+} ions on the Rb nuclei. Experimentally, this field is defined as

$$B_{eff} = B_{res} - \nu/\gamma - \Delta\nu^q/\gamma, \quad (3)$$

where $\Delta\nu^q$ is the quadrupole shift of the resonance field.

At any finite temperature the magnetic structure can be represented as a superposition of the ferromagnetic and collinear (UUD) states with the corresponding weights $\mu - \eta/3$ and η , respectively. Therefore, the effective field B_{eff} consists of two components, one of them being proportional to μ and the other being proportional to $\eta(T)$. The order parameter is hence given by the expression

$$\eta(T) \sim B_{eff}(T) - B_{eff}(T_0)M(T)/M(T_0), \quad (4)$$

where T_0 is a fixed temperature above the ordering temperature T_N . From this expression, by using the independently measured temperature dependence of the magnetic moment, one can determine the order parameter. Figure 9 gives the temperature dependence of the NMR resonance field as well as of the magnetic moment $M(T)$ measured in a field of ≈ 6 T. Figure 10 shows the temperature dependence of the order parameter obtained using the data of Fig. 9 as described above. An absolute value of the order parameter is obtained by using the results of Ref. 16, where the value of η was determined for $T = 1.6$ K and a magnetic field of 6 T. An abrupt change in the order parameter is clearly seen near the ordering temperature.

C. Magnetic phase diagram

Figure 11 summarizes the positions of the phase boundaries in $\text{RbFe}(\text{MoO}_4)_2$ for a field applied in the basal plane of the crystal, determined by using different methods. In weak fields, the transition temperature is well defined (with the accuracy better than 0.1 K) from the magnetization and specific heat measurements. The phase boundary between the paramagnetic and the collinear phase ($P3$ in Fig. 11) is also

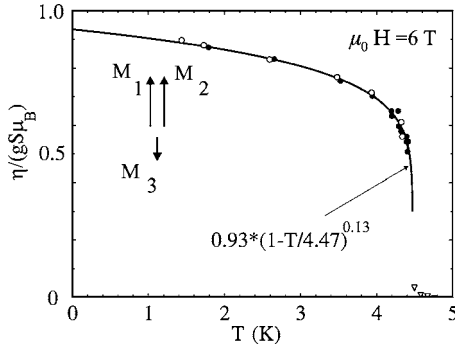


FIG. 10. Temperature dependence of the order parameter η . The solid and open circles correspond to the values of η obtained from the resonance fields of ^{87}Rb residing in different positions with respect to the magnetic structure. The triangles correspond to the values of η in the paramagnetic phase. $\mu_0 H \approx 6$ T, $\mathbf{H} \perp C_3$.

well defined by the peak in the specific heat and by the splitting in the NMR spectrum, while the magnetization curve shows a smooth behavior. The phase boundaries corresponding to the transition fields H_{c2} and H_{c3} are only visible in the magnetization curves, whereas the anomaly at H_{c1} is clearly seen in both the specific heat and the magnetization curves.

The dashed lines in Fig. 11 represent the phase boundaries obtained in our earlier paper.¹² Although the overall agreement between the two sets of the results is good, a noticeable difference between the transition temperatures is most likely to be caused by the variations in sample quality, originating from difference in the sample preparation procedures. The specific heat peaks associated with the phase transition from the paramagnetic to the collinear phase were much sharper for the new batch of samples, for which the NMR signal splitting also occurs over a narrower temperature interval. During the measurements with different samples from the same growth batch it has been noticed that by rigidly gluing the NMR sample to a sample holder it was possible to broaden significantly the phase transition region. In addition,

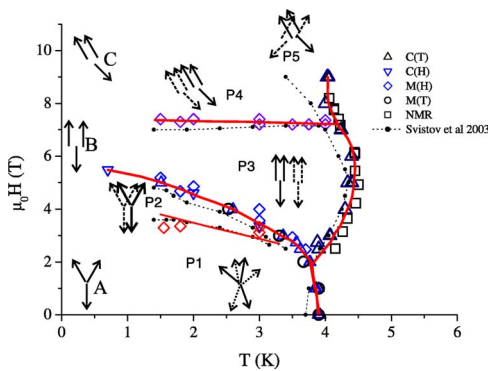


FIG. 11. (Color online) Magnetic phase diagram of $\text{RbFe}(\text{MoO}_4)_2$ for $\mathbf{H} \perp C_3$ determined by using different experimental methods. Spin structures of magnetic layers are schematically presented by solid arrows and marked as A, B, and C. Two-layer fragments of supposed 3D spin structures are shown by solid and dashed arrows for different magnetic phases marked as P1–P5; see text.

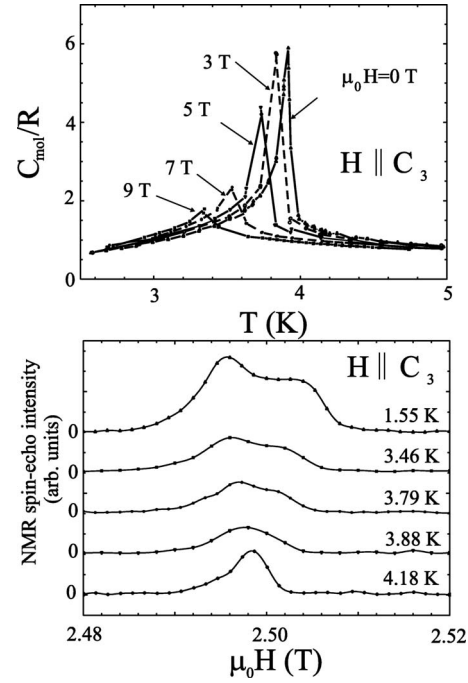


FIG. 12. Temperature dependence of the specific heat in different fields (top panel) and spectra of the central quadrupole-split NMR line measured at 35 MHz for different temperatures (bottom panel). The field is applied along the C^3 axis of the $\text{RbFe}(\text{MoO}_4)_2$ single crystal.

the specific heat measurements (performed as usual for the heat-pulse method with the crystals attached rigidly to a platform using a low-temperature grease) show that the peaks in $C(T)$ measured for the PM to P3 transition in the thinner and therefore more stressed samples were about 0.2 K broader compared to the thicker and less stressed samples. It should be added, however, that the shape and the width of the peaks in $C(T)$ curves were not sensitive to the stress for the other magnetic phases (above and below the phase with a collinear structure).

IV. MAGNETIC PHASE DIAGRAM FOR $\mathbf{H} \parallel C^3$

Figure 12 (upper panel) shows the temperature dependence of the specific heat measured in $\text{RbFe}(\text{MoO}_4)_2$ for $\mathbf{H} \parallel C^3$. The lower panel also shows the records of the central quadrupolar-split NMR line measured at 35 MHz for the same direction of the field. When the field is applied along the C^3 axis (“hard” axis in terms of the magnetic anisotropy), a single phase transition into a magnetically ordered phase is observed via a λ -like anomaly in $C(T)$. This transition is seen as a sharp maximum in the $C(H)$ curves (not shown) and also as a splitting of the NMR line. For $\mathbf{H} \parallel C^3$, this splitting is nearly an order of magnitude smaller compared to the $\mathbf{H} \perp C^3$ geometry.

The H - T phase diagram for a field applied along the C^3 axis is shown in Fig. 13. The circles correspond to the phase boundary positions obtained from the specific heat measurements, while the square marks the phase transition observed by the NMR splitting.

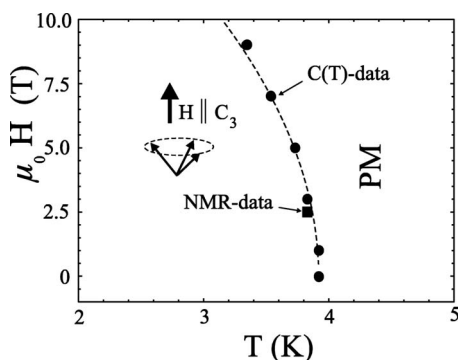


FIG. 13. The magnetic phase diagram of the $\text{RbFe}(\text{MoO}_4)_2$ single crystal for $\mathbf{H} \parallel C^3$. The dashed line corresponds to the relation $\mu_0 H = 20.2 \text{ T} \times (1 - T/3.9 \text{ K})^{0.5}$. The value of the experimental uncertainty in the position of the phase boundary is represented by the markers' size.

V. DISCUSSION

A. Initial aspects

Here we discuss the observed phase transitions in $\text{RbFe}(\text{MoO}_4)_2$ and its critical properties. Apart from the data presented in this paper, the discussion will be based on the available data on the microscopic structure of $\text{RbFe}(\text{MoO}_4)_2$ obtained from neutron diffraction¹⁵ and NMR¹⁶ experiments, as well as on the established hierarchy of the magnetic interactions:¹² the intralayer exchange, the easy-plane anisotropy, and the interlayer exchange. Besides these experimental facts we shall use the results of the calculation of the dipole energy, which can help to select between the proposed states with equal nearest-neighbor exchange energy.

It has to be noted that in zero field and at finite temperature for the case of an ideal two-dimensional system, long-range order of the magnetic components is prohibited by the Mermin-Wagner theorem. For a triangular lattice with antiferromagnetic exchange interactions, however, apart from the Berezinskii-Kosterlitz-Thouless transition there should be an additional transition to a state with long-range order with the chirality parameter for the neighboring triangles, the so-called “staggered helicity (vorticity)” state.^{8,9} Monte Carlo simulations for this state⁹ show that this phase is close to the state with long-range order of the nonzero average magnetic moments, as the spin-spin correlations decay in a power-law manner. Moreover, the characteristic relaxation time for the 120° three-sublattice structure could be relatively long and may exceed the dynamical range for various experimental techniques.

Computer simulations show the presence of chiral ordering both for the 2D XY model⁴ and 2D Heisenberg system.^{9,17} For the 2D XY model, in addition to the paramagnetic phase, the H - T phase diagram contains the three ordered phases,⁴ which have previously been identified in, for example, Ref. 8. These structures are depicted and labeled as A , B , and C in Fig. 11.

In the presence of an external magnetic field, the stabilization of long-range order becomes inevitable.⁸ Computer simulations for the Heisenberg spins^{9,17} reveal qualitatively similar results to the XY -model phase diagram; however, the

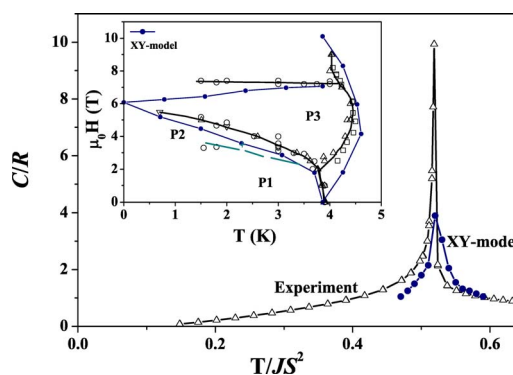


FIG. 14. (Color online) Experimental (open symbols) and theoretical (Ref. 4) (solid symbols) temperature dependence of the specific heat in $\text{RbFe}(\text{MoO}_4)_2$ plotted against the normalized temperature in zero field. The inset shows the H - T phase diagram for $\mathbf{H} \perp C^3$, where the open symbols represent the experimental results as in Fig. 11; solid symbols are the results of computer simulations (Ref. 4) with $J = 1.23 \text{ K}$. The solid lines in the inset are drawn as a guide to the eye.

exact positions of the phase boundaries are determined there far less accurately. Both models predict a characteristic non-monotonic variation of the ordering temperature with the magnetic field. The simulation results for the XY model are shown in Fig. 14.

Weak interlayer exchange coupling should, in the general case, facilitate the appearance of 3D long-range order. Given the results for the 2D models discussed above and the proximity of the ground states for these systems, one can speculate that the temperature of the 3D ordering should be close to the critical temperature of the 2D transition. In order to corroborate this conjecture, additional Monte Carlo simulations for the system with a finite interlayer exchange and magnetic anisotropy would be required.

In order to analyze the real structures in 3D crystals one has to take into account the interlayer exchange coupling and to consider various possibilities for the alignment of the spins in the neighboring planes. Theoretical analysis of the different allowed structures for an antiferromagnetic interlayer exchange has been performed in Ref. 6. The proposed magnetic phases have then been used as the models for $\text{RbFe}(\text{MoO}_4)_2$ in Ref. 12. Figure 11 shows the spin configurations of the ordered phases, which have been selected from the proposed list⁶ on the basis of matching the NMR-detected commensurate-incommensurate transition,¹⁶ magnetization plateau, and possible periodicity along C^3 direction, which is discussed below. Solid and dashed arrows in Fig. 11 represent the orientations of the magnetic moments of the Fe^{3+} ions from neighboring planes for these selected configurations.

Let us consider the procedure of the selection of the proposed structures. One should note that for the spin structures with two parallel sublattice magnetizations within a layer (e.g., structures suggested for phases $P2$, $P3$, and $P4$), an interlayer exchange does not define the magnetic periodicity along the C^3 axis, which could therefore be any integer multiple of the lattice periods. This point is illustrated in Fig. 15, where the two structures with the periodicity along the C^3

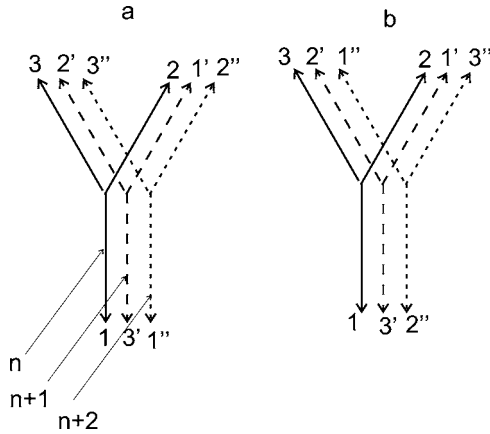


FIG. 15. Schematic representation of the magnetic structures with different periodicity along the C^3 axis: $2c$ on the left (a) and $3c$ on the right (b). Solid and dashed arrows correspond to the direction of the magnetic moments in the neighboring planes. Numbers 1, 1', and 1'' mark the magnetic moments of the Fe^{3+} ions located above one another in the neighboring n th, $n+1$ st and $n+2$ nd magnetic layers.

axis equal $2c$ and $3c$ and contain the same number of various angle combinations for the neighboring spins. These two structures thus possess the same exchange energy. This periodicity must be due to some other interactions that are weaker when compared to the exchange coupling. Among the possible candidates for the interactions which select a period along C^3 axis are the dipole-dipole interactions and further neighbor exchange interactions along the C^3 axis. The direct calculation of the dipole energy shows that it is lower for the period of $3c$. This gain in the dipole energy equals approximately 0.4 mK per Fe ion for UUD structure. Therefore we suppose that the structures suggested for phases $P2$, $P3$, and $P4$ have the period $3c$. The next-nearest antiferromagnetic exchange interaction in the C^3 direction would also result in the preference of period $3c$.

Figure 11 shows results of the various experimental techniques that reveal the presence of five ordered phases. The phase transition, corresponding to the field H_{c3} , which is marked in the $\frac{dM}{dH}$ curves in Fig. 2, is an incommensurate-commensurate transition indicated by the characteristic change of the NMR spectrum.¹⁶ We suppose that the incommensurate structure below H_{c3} corresponds, as usual, to a nearly antiparallel orientation of spins from neighboring layers (structure $P1$), this structure being rotated around the C^3 axis by a small angle from layer to layer. In the range above H_{c3} the commensurate structure takes place for the phase $P2$. In Ref. 12, two possible variants were proposed for the spin structures in phases $P1$ and $P2$ based on the results of theoretical considerations.^{6,18} We selected for the phase $P2$ the structure which allows the period of $3c$, favorable for dipole-dipole energy. For the phase $P1$ the structure, compatible with period $2c$ is suggested, since for the typical incommensurate structures in antiferromagnets the orientation of spins in neighboring layers should be close to an antiparallel one, like at the period value $2c$.

In the phase $P3$ —i.e., in the plateau range—the collinear structure within a layer and the periodic structure along C^3

axis, probably with the period $3c$, is realized. The structures of $P4$ or $P5$ type may be proposed for the high-field range between H_{c2} and saturation. We have here no NMR data which could distinguish between commensurate and incommensurate states; thus, we cannot determine the nature of the $P4$ - $P5$ boundary, detected by a small dM/dH singularity in Ref. 12. Nevertheless, if we extrapolate the period value of $3c$ from $P3$ to $P4$, the structure which is compatible with period $3c$ should be selected, as shown in Fig. 11. In this case the transition to the second high-field spin structure of the phase $P5$ should change the period to $2c$ or again result in the incommensurate modulation.

The collinear structure of the $P3$ phase may be taken as determined most precisely, as it corresponds to the maximum value of the NMR shift,¹⁶ which is maintained in the entire field range $H_{c1} < H < H_{c2}$. The spin structures of other phases are suggested as probable configurations.

B. 2D-3D crossover of the specific heat temperature dependence

The overall shape of the phase diagram, as well as the characteristic widening of the collinear phase range with increasing temperature predicted in Ref. 8, points to the two-dimensional nature of magnetism in $\text{RbFe}(\text{MoO}_4)_2$. Here, we show that the observed change-over in the temperature dependence of the specific heat from the low-temperature T^3 law to the intermediate temperature T^2 law (as described in Sec. III A) is also indicative of the two-dimensional disposition of this magnetic system.

The temperature dependence of the specific heat of an antiferromagnet for $T < 0.6 T_N$ is usually determined by thermally activated magnons. The spectrum of acoustic magnons in antiferromagnetic $\text{RbFe}(\text{MoO}_4)_2$ consists of one gapless mode and two modes with a gap of 90 GHz (4.5 K).¹² At such low temperatures, the variation of the gap's magnitude should be small, as the order parameter for $T < 0.6 T_N$ is reduced by not more than 30% . The main contribution to the specific heat in this temperature region comes from the magnons of the gapless branch. At the lowest temperature the wave numbers of the thermal magnons are small and lie far away from the Brillouin zone boundary. Therefore one can expect for $C(T)$ a typical three-dimensional behavior—that is, $C(T) \sim T^3$.

Due to a large difference between the interlayer and intralayer exchange interactions, the magnon dispersion relation is highly anisotropic—the magnons propagating along the C^3 axis are less dispersive than those with a wave vector confined to the triangular plane. Consequently, at a certain temperature, the energy of the thermal magnons traveling along the C^3 axis reaches its maximum value, while the size of the k -space region corresponding to magnons with $k \perp C^3$ will continue to expand. For these temperatures one can expect a typical two-dimensional behavior—that is, $C(T) \sim T^2$. Inevitably, the change over from a cubic to a quadratic law should occur at the temperature dependent on interlayer exchange energy or, more precisely, on the maximum energy of the $k \parallel C^3$ magnons of the lowest gapless branch. This is the energy of the lowest “exchange” mode of the antiferromagnetic

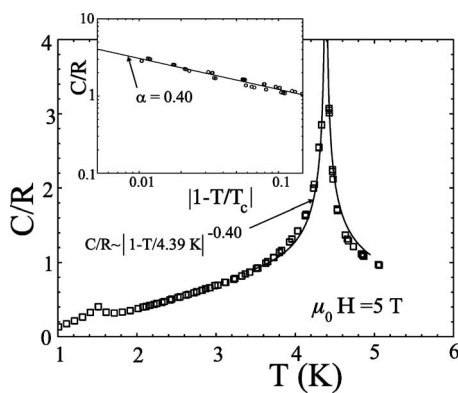


FIG. 16. Temperature dependence of the specific heat for a field of $\mu_0 H = 5$ T applied in the easy plane of $\text{RbFe}(\text{MoO}_4)_2$. The inset shows the C vs $|1 - T/T_c|$ curve in the vicinity of the phase transition on a log-log scale.

resonance spectrum. According to Ref. 12, the gap of the lowest exchange mode is about 30 GHz (1.5 K), which agrees well with the observed crossover temperature. Thus the 2D-3D crossover in the temperature dependence of specific heat confirms the domination of two-dimensional features in the thermodynamic behavior of $\text{RbFe}(\text{MoO}_4)_2$.

C. Critical properties of the magnetic ordering transition for $\mathbf{H} \perp \mathbf{C}^3$

Given the two-dimensional nature of the magnetic properties of $\text{RbFe}(\text{MoO}_4)_2$, let us compare the observed critical behavior with the results of the classical Monte Carlo simulations⁴ performed for the 2D XY model. The Néel temperature in this simulation is defined as $0.5JS^2$. Using the value of $J = 1.2 \pm 0.1$ K determined from the susceptibility and saturation magnetization measurements,^{12,13} the predicted ordering temperature is 3.75 ± 0.3 K, which is in a good agreement with the value of $T_N = 3.85 \pm 0.05$ K determined experimentally. The ordering temperature for the 2D Heisenberg antiferromagnet on a triangular lattice, on the other hand, is defined as $0.35JS^2$,¹⁷ which unexpectedly gives less satisfactory agreement with the experimental T_N .

Figure 14 shows the comparison between the temperature dependence of the specific heat measured experimentally and obtained from the Monte Carlo simulations.⁴ It also shows a comparison of the phase boundary positions from the experimental H - T diagram (see Fig. 11) and the simulations⁴ for $\mathbf{H} \perp \mathbf{C}^3$. For the theoretical curve, the value of the exchange parameter quoted above has been used. The overall agreement is satisfactory, as the two phase diagrams have very similar shapes, apart from the low-field region. For low fields, however, the distinction is fundamental: the theoretical model predicts a phase transition from paramagnetic to chiral structures only through a collinear phase, while experimentally a single phase transition is observed for all fields below 2 T.

The measured $C(T)$ and $\eta(T)$ curves allow one to evaluate the specific heat and the order parameter critical indices for the phase transition into the collinear phase. Corresponding experimental data are presented in Figs. 10 and 16. The ex-

perimentally determined indices are $\alpha = 0.40 \pm 0.03$ for the specific heat and $\beta = 0.13 \pm 0.02$ for the order parameter. They agree well with $\alpha = 1/3$ and $\beta = 1/9$ obtained from the simulations.⁴ Because of the very steep dependence of the order parameter in the vicinity of T_N , it is impossible to get a set of experimental points in the range where the order parameter is smaller than one-half of a nominal value. Thus, the obtained values of the critical indices β and α should be taken as evaluations.

It can be concluded then that the ordering temperature, the magnetic phase diagram, and the critical indices of the specific heat and the order parameter demonstrate a satisfactory quantitative agreement with the 2D XY -model predictions for zero field and also for regions of the field ($\mathbf{H} \perp \mathbf{C}^3$) where the collinear phase is stable. Most likely this agreement can be explained by the large value of the energy gap for the magnon branch, which corresponds to a deviation of the spins out of the basal plane.

This gap has been estimated as 90 GHz (or 4.3 K).¹² Therefore, for all the magnetically ordered phases, the thermodynamic properties are defined by gapless and low-energy magnons, corresponding to spin fluctuations within the easy plane. This, in turn, justifies the applicability of the XY model.

D. Phase diagram for $\mathbf{H} \parallel \mathbf{C}^3$

The easy-plane type of magnetic anisotropy in $\text{RbFe}(\text{MoO}_4)_2$ is confirmed by the observation of the magnetization plateau around $M_s/3$ for the magnetic field applied in the ab plane and by the linear rise of the $M(H)$ curves for the field parallel to the \mathbf{C}^3 axis. For an easy-plane anisotropy, the magnetic moment of the system is generated for $\mathbf{H} \parallel \mathbf{C}^3$ by the even tilts of all the sublattices in an umbrella-like structure towards the field (see Fig. 13). For such a system, the application of an external magnetic field should result in a decrease of the ordering temperature. Moreover, in the vicinity of $T_N(H=0)$, the reduction should be proportional to the square of the field, similarly to an ordinary two-sublattice antiferromagnet.¹⁹ The dashed line in Fig. 13 shows such a dependence $H_c = a(1 - T/T_c)^{0.5}$, with $a = 20.2$ T and $T_c = 3.9$ K. For the case of the uniformly tilted spins described here, splitting in the NMR spectra should be absent, but it is observed. The origin of this small but clearly visible splitting remains unknown at the present time.

VI. CONCLUSIONS

To summarize, we have performed a systematic and comprehensive study of the thermodynamic and magnetic properties of the quasi-two-dimensional TLAM $\text{RbFe}(\text{MoO}_4)_2$, as well as measurements of the magnetic order parameter for this compound. A crossover from a T^2 law to a T^3 law is observed for the temperature dependence of the specific heat at low temperatures. The phase diagram and critical properties demonstrate a surprisingly good quantitative agreement with the predictions for the XY model despite the fact that the easy-plane anisotropy in $\text{RbFe}(\text{MoO}_4)_2$ does not dominate the main exchange interaction.

ACKNOWLEDGMENTS

The authors are grateful to S.E. Korshunov, V.I. Marchenko, M.E. Zhitomirsky, A. Loidl, and H.-A. Krug von Nidda for discussions and to M.R. Lees for a critical reading of the manuscript. This work is supported by Grant No. 04-

02-17294 of the Russian Foundation for Basic Research, RF President Science Schools Program, Contract No. BMBF VDI/EKM 13N6917-A, program of the German research society Sonderforschungsbereich 484 (Augsburg), and the EPSRC grant (University of Warwick). The work of L.E.S. is supported by the Alexander von Humboldt Foundation.

-
- ¹M. F. Collins and O. A. Petrenko, *Can. J. Phys.* **75**, 605 (1997).
²S. Nakatsuji, Y. Nambu, H. Tonomura, O. Sakai, S. Jonas, C. Broholm, H. Tsunetsugu, Y. Qiu, and Y. Maeno, *Science* **309**, 1697 (2005).
³H. Kawamura, *J. Phys. Soc. Jpn.* **54**, 3220 (1985).
⁴D. H. Lee, J. D. Joannopoulos, J. W. Negele, and D. P. Landau, *Phys. Rev. B* **33**, 450 (1985).
⁵A. V. Chubukov and D. I. Golosov, *J. Phys.: Condens. Matter* **3**, 69 (1991).
⁶R. S. Gekht and I. N. Bondarenko *Zh. Eksp. Teor. Fiz.* **111**, 627 (1997) R. S. Gekht and I. N. Bondarenko, [*JETP* **84**, 345 (1997)].
⁷E. Rastelli and A. Tassi, *J. Phys.: Condens. Matter* **8**, 1811 (1996).
⁸S. E. Korshunov, *J. Phys. C* **19**, 5927 (1986).
⁹H. Kawamura and S. Miyashita, *J. Phys. Soc. Jpn.* **53**, 4138 (1984).
¹⁰R. F. Klevtsova and P. V. Klevtsov, *Kristallografiya* **15**, 953 (1970).
¹¹S. A. Klimin, M. N. Popova, B. N. Mavrin, P. H. M. van Loosdrecht, L. E. Svistov, A. I. Smirnov, L. A. Prozorova, H.-A. Krug von Nidda, Z. Seidov, A. Loidl, A. Ya. Shapiro, and L. N. Demianets, *Phys. Rev. B* **68**, 174408 (2003).
¹²L. E. Svistov, A. I. Smirnov, L. A. Prozorova, O. A. Petrenko, L. N. Demianets, and A. Ya. Shapiro, *Phys. Rev. B* **67**, 094434 (2003).
¹³T. Inami, Y. Ajiro, and T. Goto, *J. Phys. Soc. Jpn.* **65**, 2374 (1996).
¹⁴G. A. Jorge, C. Capan, F. Ronning, M. Jame, M. Kenzelmann, G. Gasparovich, C. Broholm, A. Ya. Shapiro, and L. N. Demianets, *Physica B* **354**, 297 (2004).
¹⁵G. Gasparovich, M. Kenzelmann, C. Broholm, L. N. Demianets, and A. Ya. Shapiro (private communication).
¹⁶L. E. Svistov, L. A. Prozorova, N. Buttgen, A. Ya. Shapiro, and L. N. Dem'yanets, *JETP Lett.* **81**, 102 (2005).
¹⁷H. Kawamura and S. Miyashita, *J. Phys. Soc. Jpn.* **54**, 4530 (1985).
¹⁸S. E. Korshunov (private communication).
¹⁹E. M. Lifshitz, L. D. Landau, and L. P. Pitaevskii, *Electrodynamics of Continuous Media, Landau and Lifshitz Course of Theoretical Physics*, Vol. 8 (Butterworth-Heinemann, Oxford, 1995).